Energy Conversion and Management 302 (2024) 118137

Contents lists available at ScienceDirect

Energy Conversion and Management

journal homepage: www.elsevier.com/locate/enconman

Research Paper

Machine learning-based multi-objective optimization of concentrated solar thermal gasification of biomass incorporating life cycle assessment and techno-economic analysis

Yi Fang [a], Xian Li [b], Xiaonan Wang [c], Leilei Dai [d], Roger Ruan [d], Siming You [a,*]

[a] James Watt School of Engineering, University of Glasgow, Glasgow G12 8QQ, UK
[b] Institute of High Performance Computing (IHPC), Agency for Science, Technology and Research (A*STAR), 1 Fusionopolis Way, #16-16 Connexis, Singapore 138632, Republic of Singapore
[c] Department of Chemical Engineering, Tsinghua University, Beijing 100084, China
[d] Center for Biorefining and Department of Bioproducts and Biosystems Engineering, University of Minnesota, 1390 Eckles Ave., St. Paul, MN 55108, USA

ARTICLE INFO

Keywords:
Biomass
Concentrated solar thermal energy
Gasification
Life cycle assessment
Techno-economic analysis
Multi-objective optimization

ABSTRACT

The combination of solar and biomass energy systems is regarded as a highly promising technology for tackling the challenges related to greenhouse gas emissions from energy generation and the increasing costs of energy production. This research centers on an integrated solar-bioenergy system, which includes a concentrated solar tower, thermal energy storage, and a combined cycle gas turbine. The system was evaluated using a multi-objective optimization approach considering life cycle assessment and cost-benefit analysis. The long short-term memory recurrent neural network algorithm with 5.1 % average error had been employed to capture the intricate temporal dependencies and dynamics of the system. The scenarios are expanded by using the Monte Carlo approach to address the challenges of limited specialized models and experiments for the system. The optimal solution is determined through the technique for order preference by similarity to ideal solution method. Carbon tax significantly influenced the results of the multi-objective optimization. The optimal configuration of the system could avoid the trade-off phenomenon when treating the carbon tax as revenue. The best scenario of the system with the cumulative reduction in global warming potential amounted to 415,960 tons of CO_2-eq and a 30-year net present worth of €4,298 million. Without considering the carbon tax as revenue, the trade-off is present. The best scenario of the system with the cumulative reduction in global warming potential amounted to 132,615 tons of CO_2-eq and net present worth of €3,042 million. The findings highlight the robust prospects of the system across environmental and economic dimensions.

1. Introduction

Faced with the global challenges of fossil fuel depletion and increasing greenhouse gas (GHG) emissions, the concentrated solar thermal gasification of biomass (CSTGB) system, as an innovative renewable energy technology, has shown tremendous potential [1]. Fang *et al.* [2] showed that CSTGB systems could enhance the utilization efficiency of biomass feedstock by 25–50 % and achieve significant reduction in the emission of pollutants (*i.e.,* NO_x, PM_{10}, and VOCs) compared to other conventional bioenergy processes.

The in-depth analysis of the CSTGB system based on the approaches, *e.g.*, life cycle assessment (LCA) [3] and techno-economic assessment (TEA), is desired for evaluating the feasibility of CSTGB development, with the highlighting of its potential environmental and economic benefits. A recent LCA and TEA study [4] introduced a thermal energy storage (TES) system in CSTGB and implemented a strategy of combusting a portion of the feedstock during nighttime or periods of low solar radiation to address the intermittency of solar energy. This strategy allows the CSTGB system to utilize the solar thermal energy collected during the day for gasification reaction even at night, leading to a significant reduction in carbon emissions. It was shown that the CSTGB system equipped with a carbon capture and storage (CCS) could reduce CO_2 emission by 787.7 kg of CO_2-eq/$ton_{waste\text{-}wood}$, while also generating about 0.8 million MWh of electricity annually. The computed net present worth (NPW) for the system was about €–0.7 billion. This economics of the CSTGB development was closely linked to the constraints imposed by existing environmental emission regulations (*i.e.,* carbon

* Corresponding author.
E-mail address: siming.you@glasgow.ac.uk (S. You).

https://doi.org/10.1016/j.enconman.2024.118137
Received 28 October 2023; Received in revised form 2 January 2024; Accepted 22 January 2024
Available online 31 January 2024

Nomenclature

kW	Kilowatt
kWh	Kilowatt-hour
MWh	Megawatt-hour
Nm^3	Normal cubic meter
N	Operation years

Abbreviation

AW	Annual Worth
CAPEX	Capital Expenditure
CCS	Carbon Capture and Storage
CCGT	Combined Cycle Gas Turbine
CO_2-eq	Carbon Dioxide Equivalent
CST	Concentrated Solar Tower
CSTGB	Concentrated Solar Thermal Gasification of Biomass
CT	Carbon Tax
DNI	Direct Normal Irradiation
ES	Electricity Selling
GHG	Greenhouse Gas
GWP	Global Warming Potential
LCA	Life Cycle Assessment
LCI	Life Cycle Inventory
LCIA	Life Cycle Impact Assessment
LHV	Low Heating Value
LSTM	Long Short-Term Memory
MOO	Multi-Objective Optimization
MSE	Mean Squared Error
NPW	Net Present Worth
O&M	Operational and Maintenance
PW	Present Worth
RNN	Recurrent Neural Network
SOO	Single-Objective Optimization
STM	Screw Transfer Machine
TEA	Techno-Economic Analysis
TES	Thermal Energy Storage
TOPSIS	Technique for Order Preference by Similarity to Ideal Solution

tax) and electricity prices.

The approaches of multi-objective optimization (MOO) can be utilized to delicately balance between environmental sustainability and economic viability [5]. The pareto optimal solution is obtained based on MOO, which can be combined with the technique for order of preference by similarity to ideal solution (TOPSIS) methods to choose the best solution [6]. The integrated framework aids in identifying the best compromise solutions among multiple objectives, thereby enhancing the efficiency and effectiveness of decision making.

The application of advanced data analysis and modelling techniques can facilitate the making of complex decisions. Complex energy systems like CSTGB integrated with TES and CCS, sophisticated data processing and pattern recognition approaches are desirable. Among existing approaches, long short-term memory (LSTM) - recurrent neural networks (RNN) represents a promising option in modelling the complex interactions within the CSTGB system. In particular, the LSTM-RNN model is proficient at capturing the dynamic and temporal patterns in energy systems, favoring more precise and effective optimizing of the system [7]. For example, Bouktif *et al.* [8] explored the use of LSTM-RNN modelling for energy yield forecasting in solar thermal energy system. Their study aimed to find the balance between performance, cost, and environmental impacts and highlighted that the importance of optimal LSTM configuration for capturing energy consumption patterns and revealing time-series dynamics (*i.e.,* DNI). Pravin *et al.* [9] expanded the application scope of LSTM-RNN modelling to study an integrated energy system. This system integrates solar energy with waste-to-energy production for enhanced electricity generation. Their study emphasized the necessity of identifying the optimal hyperparameter configuration based on the dual criteria of minimum validation mean squared error (MSE) and computational efficiency (epochs).

The application of LSTM-RNN model as a data-driven tool has been demonstrated, albeit limited to system modeling [10]. The persistent challenge on the application of LSTM-RNN to model CSTGB lies in the data availability as there are limited data, especially experimental data about the development of CSTGB. In this case, the Monte Carlo simulation approach can be applied to enrich the dataset, with the potential to enhance the robustness of MOO in the analysis of the CSTGB system. The effectiveness of the use of Monte Carlo simulation on supporting the development of LSTM-RNN modelling for CSTGB awaits to be examined.

This study introduced an approach to address the challenge surrounding the optimisation of CSTGB system incorporating LCA and TEA: a data-driven MOO approach that encompassed both environmental and economic considerations was proposed and tested to optimize the design and operation of CSTGB. The LSTM-RNN model was utilized to capture the intricate temporal dependencies and dynamics associated with the development of a CSTGB system while Monte Carlo simulation was applied to expand the dataset for model training. The optimal compromise solutions that strike a balance between conflicting objectives, namely, minimizing environmental impacts and maximizing economic benefits were revealed. Overall, a comprehensive framework was proposed to holistically optimize the CSTGB system, offering insights into its feasibility, sustainability, and potential for the best implementation.

2. Methodology

The schematic diagram of the illustration of the methodology is depicted in Fig. 1, including CSTGB system performance evaluation, LCA, TEA, the integration of the LSTM-RNN model with Monte Carlo approach, and MOO with pareto optimal solution and TOPSIS methods. This optimization framework comprehensively addressed various facets, including electricity generation, carbon capture efficiency, environmental feasibility, and economic viability.

Initiating the system design phase, a preliminary thermodynamic analysis was conducted to ascertain crucial gasifier specifications, encompassing parameters such as reaction temperature, thermal energy demand, and air-to-feedstock ratio (it refers to the ratio between the mass of air and that of the feedstock (*i.e.,* biomass waste) supplied to the gasifier). Concurrently, the SolarPILOT software [11] was applied in defining parameters for solar heliostats, including the layout and area, specifications of the CST receiver, and encompassing factors (*e.g.,* receiver surface area and tower height). Building upon these foundational design parameters in our previous study [4], the optimal process conditions for achieving maximum electricity generation in a single scenario and life cycle inventory (LCI) data were determined through single-objective optimization (SOO).

The LSTM-RNN model was seamlessly integrated into the methodology, infusing a heightened level of effective decision-making capability [12]. The LSTM-RNN model was trained on operational data and patterns from 125 scenarios. Each scenario encompassed variations in biomass feedstocks, geographical locations, and reaction temperatures. Subsequently, we established a dynamic data augmentation by synergizing the predictive ability of the LSTM-RNN model with the stochastic nature of the Monte Carlo approach. This was achieved by stochastically selecting feature parameters within pre-defined ranges (as mentioned in

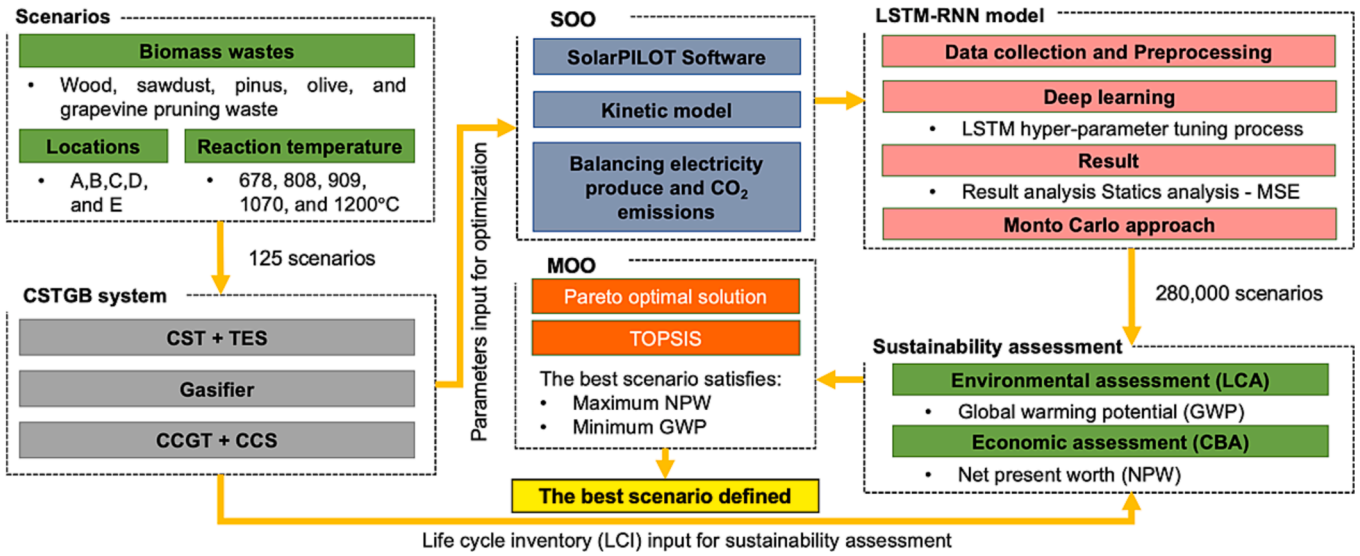

Fig. 1. Schematic illustration of the proposed methodology. CSTGB: concentrated solar thermal gasification of biomass; CST: concentrated solar tower; TES: thermal energy storage; CCGT: combined cycle gas turbine; CCS: carbon captured system; SOO: single-objective optimization; MOO: multi-objective optimization; TOPSIS: technique for order of preference by similarity to ideal solution; LSTM-RNN: long short-term memory recurrent neural network; MSE: mean squared error.

Section 2.4). The introduction of this stochastic element led to the generation of new instances rooted in the inherent system dynamics while considering a broader spectrum of potential scenarios. It was noteworthy that this integrated approach swiftly broadens the dataset, transforming it from the initial set of 125 scenarios into an extensive collection comprising 280,000 scenarios.

The operational parameters and system configurations (*i.e.,* LCI) obtained from the extensive collection of generated scenarios were merged and utilized as inputs for both LCA and TEA. These evaluations not only encompassed the assessment of the GWP but also rigorously evaluated the economic feasibility (*i.e.,* NPW) of CSTGB system. The pareto optimal solution and TOPSIS approaches ensure that the outcomes of the MOO satisfy both environmental and economic objectives, thus fostering a well-informed decision-making framework at the confluence of green technology and economic viability.

2.1. Overview of the CSTGB system

The specific parameter design of the CSTGB system was provided in the previous study [4]. The CSTGB system employs a synergistic thermal energy approach, in which thermal energy derived from the combustion of feedstock, the solar thermal energy from the CST subsystem, and the thermal energy stored within the TES subsystem are complementing each other. The deliberate integration is to mitigate the adverse impact of severe weather conditions or intermittent solar thermal conditions (*i.e.,* limited solar radiation during nighttime and winter and the insufficiency of nocturnal solar irradiance) on the system's performance. Implementing this strategy enhances the system's ability to adapt and maintain consistent performance.

Fig. 2 presents a schematic illustration of the CSTGB system. The size of the heliostat field, the dimensions of the CST receiver, and the capacity of the TES subsystem in the CSTGB system (as shown in Table 3) were decided according to the regional DNI and the specific temperature (*i.e.* thermal energy) demands of the gasifier. These demands involve consideration such as the temperature and heat necessary to maintain the gasification process, which converts feedstock into producer gas. A screw transfer machine (STM) was employed for conveying thermally charged quartz sand to both the TES subsystem and the internal heat exchanger of the fixed bed gasifier (details regarding the electricity consumption of the STM is shown in Table 3). This gasifier employs air as its gasifying agent, based on its lower cost. The design of CSTGB follows an indirect reactor approach, where the quartz sand and feedstock particles are kept separate and a 5 % gas leakage between the gasifier and the STM equipment is considered [13]. The high-quality producer gas, characterized by a notably elevated low heating value (LHV) by the solar thermal heating, is the principal output of the CSTGB system. This producer gas comprises a specific mix of combustible gases including carbon monoxide (CO), hydrogen (H_2), and methane (CH_4). The LHV of the producer gas is calculated as $(CO \times LHV_{CO} + H_2 \times LHV_{H_2} + CH_4 \times LHV_{CH_4})$, where CO, H_2, and CH_4 are the volume fractions of the producer gas [14]. The presence of these components in significant amounts results in a gas mixture with a suitably high energy content, making it an fuel suitable for various energy generation applications [15]. Following the removal of tar and fine particles via a gas cleaning unit, the producer gas is subsequently fed into a combined cycle gas turbine (CCGT) subsystem for electricity generation. Furthermore, the by-product (*i.e.,* CO_2) produced from the CSTGB system is captured and stored by a CCS subsystem, effectively minimizing on-site CO_2 emissions.

The performance evaluation of the CSTGB system incorporates hourly TMY data to estimate annual electricity generation and CO_2 capture. By utilizing TMY data, the analysis captures the dynamic nature

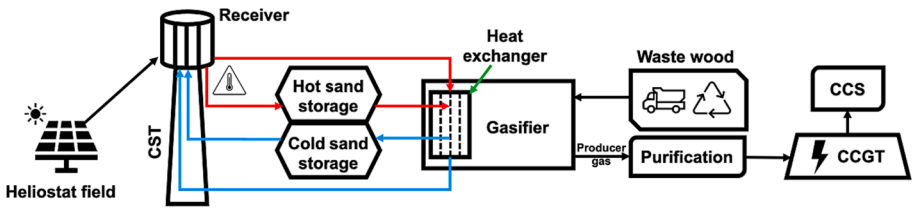

Fig. 2. The schematic diagram of the proposed CSTGB system.

of system performance under a wide range of operational and environmental conditions typical of the geographical area considered. The overall system efficiency is used to assess the energy conversion performance of the system (*i.e.,* from biomass and solar energy to electricity). The annual electricity generation and CO_2 capture are quantified through the summation of hourly data over a year.

2.2. Dataset and features description

The study initially considered 125 scenarios which were derived based on our previous research [4] which focused on the environmental and economic evaluation of the CSTGB system. Specifically, a stochastic kinetic model for the gasification process that combines a single particle shrinkage core model and Monte Carlo simulation was applied to predict the maximum producer gas yield [16]. The modelling encompassed a wide range of variables, including 5 types of biomass waste (namely wood, sawdust, pinus pruning, olive pruning, and grapevine pruning), 5 locations (labeled as A, B, C, D, and E), and 5 different gasification reaction temperatures (678 °C, 808 °C, 909 °C, 1,070 °C, and 1,200 °C). Table 1 illustrates the ultimate compositions of biomass waste that are widely available in the areas considered [17]. To ensure efficient CSTGB system operation, critical steps such as biomass waste pretreatment to maintain a moisture content below 10 % and proper sorting before transportation were considered. Table 1 also summarized the geographical characteristics (*i.e.,* latitudes, longitudes, elevations, and average DNI) of the selected locations for the development. Fig. 3 lists the TMY with hourly temporal DNI data for each location from the PVGIS database [18]. Furthermore, the distances from these locations to Seville, Spain were measured in kilometers based on the actual transportation routes marked on Google Maps. This measurement approach was incorporated into the analysis to assess the impact of the transportation distance variations on the results of LCA and TEA.

2.3. LSTM-RNN model

2.3.1. LSTM-RNN model architecture

The LSTM-RNN model is a type of deep learning architecture specifically designed to capture temporal dependencies in time series data (*e.g.,* DNI) and other selected linear features (*i.e.,* feedstock compositions and reaction temperature) and non-linear features (*i.e.,* locations) using the LSTM unit (as mentioned in Section 1). In this study, we allocated 80 % of the datasets from 125 scenarios (as mentioned in Section 2.2) for training and 20 % for testing. The model was trained using an appropriate evaluation metric (*i.e.,* MSE) to minimize the prediction errors and enhance the performance. Fig. 4 displayed the main steps of the proposed LSTM-RNN model. The tuning essential hyperparameters were set as a learning rate of 2, a batch size of 100, a number of training iterations of 75, and 8 hidden layers, to control the convergence rate, balance memory usage, and training efficiency, and ensure that the model adequately learned the underlying data patterns. The optimization algorithms (*e.g.,* stochastic gradient descent) were used to effectively adjust the model's parameters to improve its fit to the training data. The accuracy of the LSTM-RNN model was evaluated using the MSE metric, which provided a quantitative assessment of its performance and prediction reliability. Python 3.11.4 was used as the programming environment. A virtual environment was created to run the LSTM-RNN model for this study. In this virtual environment, the packages (Tensorflow, Keras, Pandas, Sklearn, Numpy, and Matplotlib) were installed.

Table 1
Feedstock compositions (dry ash free basis) and locations.

Feedstocks selection					
Component	**Wood**	**Sawdust**	**Pinus pruning**	**Olive pruning**	**Grapevine pruning**
C (wt.%)	50.31	50.26	50.55	47.50	46.97
H (wt.%)	7.82	6.14	6.12	6.00	5.80
O (wt.%)	41.77	42.20	40.2	43.66	44.49
N (wt.%)	0.10	0.07	0.45	1.06	0.67
FC (wt.%)	16.30	16.27	15.13	13.98	19.78
LHV (kJ/kg)	18.70	20.47	19.99	19.99	17.91
Location selection					
	A	**B**	**C**	**D**	**E**
Latitude	37.5	36.6	39.9	39.2	38.7
Longitude	–5.3	–5.8	–5.7	–3.3	–0.9
Elevation (m)	137.0	107.0	272.0	648.0	544.0
Distance to Seville (km)	85	130	365	450	620
Average DNI (W/m^2)	641.4	562.7	535.7	542.3	553.7

2.3.2. Evaluation of LSTM-RNN model performance

To assess the performance of the LSTM-RNN model, two pivotal metrics were utilized: MSE for model training (training-MSE) and MSE for model validation (validation-MSE) [19]. The training-MSE gauges the degree of model fit to the training dataset, and quantified through the computation of the average squared difference between the model prediction and the actual value [20]. In contrast, the validation-MSE serves as a measure of the model's generalization prowess, addressing its performance on previously unseen data instances [21]. The validation-MSE is meticulously calculated at the culmination of each training epoch, thereby facilitating the timely detection of potential overfitting or underfitting tendencies within the model [22]. These two MSE metrics [23] were computed by

$$MSE = \frac{1}{N}\sum\nolimits_{y_i} \left(y_{predict} - y_{actual}\right)^2 \quad (1)$$

2.4. Monte Carlo simulation

The minimum and maximum percentage values for each composition component (*i.e.*, carbon (C), hydrogen (H), and oxygen (O)) were chosen as the lower and upper bounds of uniform distributions used for Monte Carlo simulation. The percentage value of N is calculated by subtracting the sum of C, H, and O from 100 % (represents as $N = 100\% - (C + H + O)$, where C, H, and O are mass fractions of carbon, hydrogen, and oxygen, respectively). Within the specific ranges (as shown in Table 2) and 5 locations, a uniform distribution was selected for random allocation. This choice guarantees an equal likelihood across the defined value range of the selected decision variables under consideration [24]. The utilization of this augmented dataset facilitates a more profound exploration of the optimization process, fostering an enhanced comprehension of the intricate relationship between the selected decision variables (input) and objective (outputs).

2.5. Life cycle assessment

The international standards series ISO 14000 offers a comprehensive structure for conducting LCA, covering essential elements including principles and framework (ISO 14040), goal and scope definition and inventory analysis (ISO 14043), and requirements and guidelines (ISO 14044) [25]. The primary aim of this LCA is to evaluate the GWP associated with the CSTGB system intended for establish in Spain.

Fig. 5 delineates the boundary of the LCA, which encompasses all relevant processes within the CSTGB system. Within this LCA system boundary, several critical sub-processes are included (*i.e.,* CO_2 emission stemming from diesel refinery, onsite CO_2 emission, the carbon capture performance by the CCS subsystem, the transportation of biomass wastes, and the electricity generation realized by the proposed CSTGB system. This delineation provides a robust foundation for the systematic evaluation of the environmental impacts and sustainability

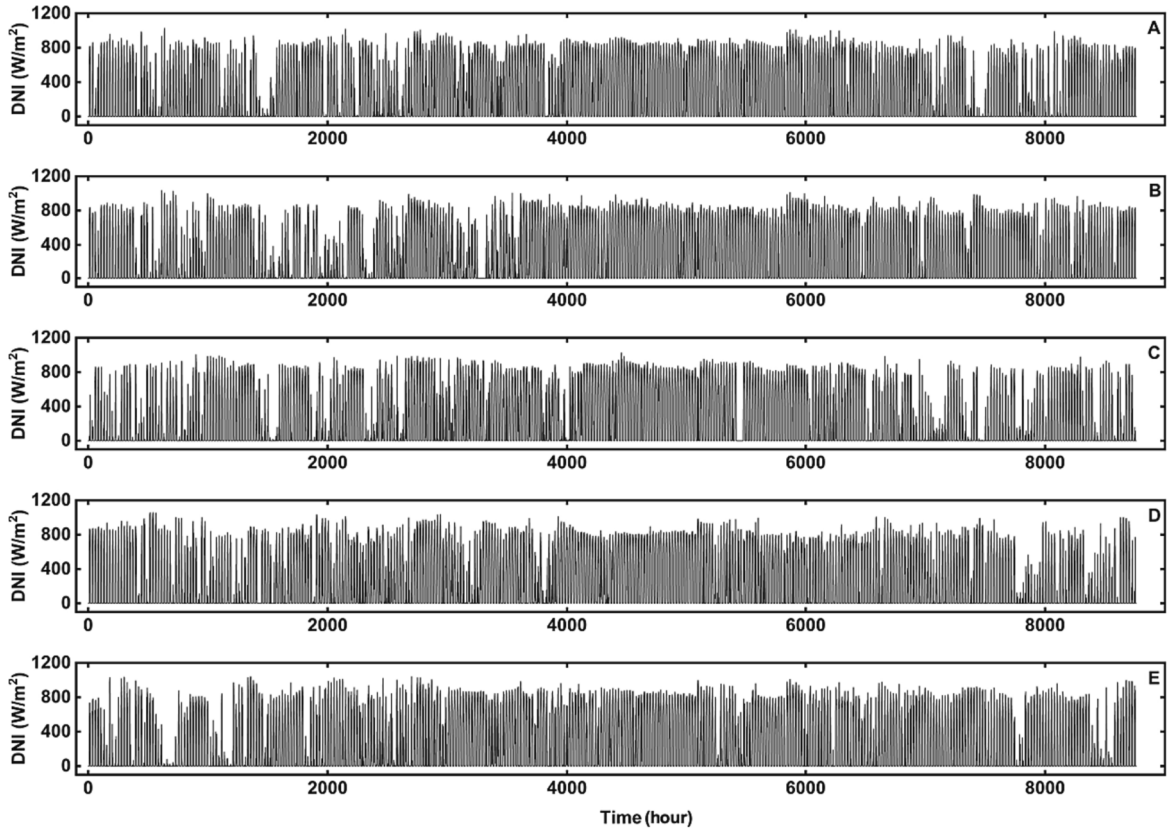

Fig. 3. Hourly DNI data profiles for locations A, B, C, D, and E.

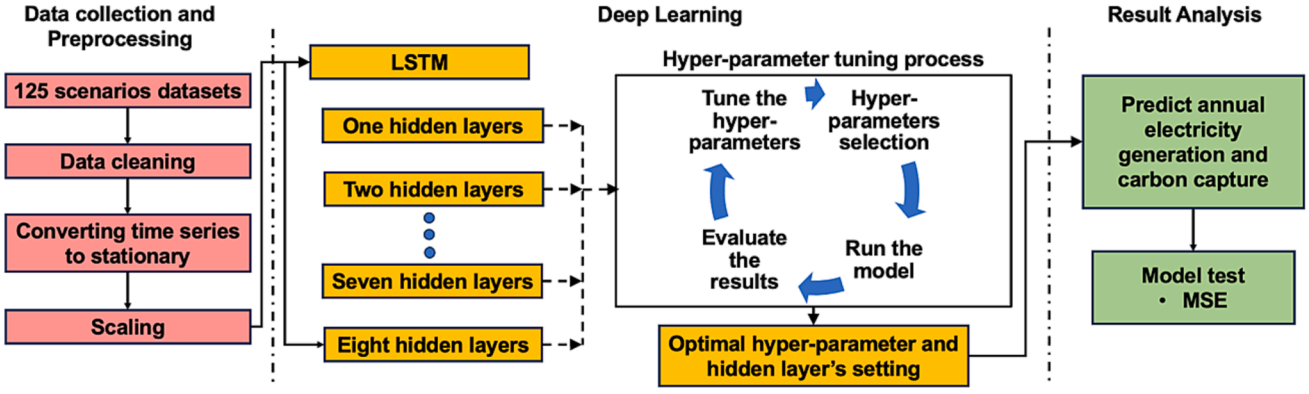

Fig. 4. Main steps of the proposed LSTM-RNN model.

Table 2
The lower and upper bounds of selected decision variables for the CSTGB system.

Variable	Lower bound	Upper bound
C (wt.%)	46.97	50.55
H (wt.%)	5.80	7.82
O (wt.%)	40.20	44.49
N (wt.%)	0.07	1.06
FC (wt.%)	13.98	19.78
LHV (kJ/kg)	17.91	20.47
Reaction temperature (Â°C)	678	1,200

consideration across the entirety of the system.

The findings of this assessment will be instrumental in planning biomass feedstocks treatment and facilitating renewable energy generation. The functional unit established for treating 1 $ton_{biomass\text{-}waste}$. Point 1 represents the diesel consumption required for transporting the biomass waste (ranging from 8 to 62 L), contingent on transportation distance (as mentioned in Section 2.2). Point 2 corresponds to the TES subsystem (storing 0.08–0.10 MWh of thermal energy) with variations based on the local DNI. Point 3 signifies electricity usage in the screw machine (a consumption of 1.0–1.1 kWh) dependent on the pipeline distance in the CSTGB system in different location. Points 4 and 5 represents the gasifier yielding 2,388–5,101 Nm^3 of producer gas, while also producing 2.2–4.6 kg of ash. The quantities of the producer gas and ash were considered to depend on multiple factors, such as the chemical composition of the feedstock and gasification process condition (*i.e.,* temperature), technical characteristics of the gasifier, and DNI. Points 6, 7, 8, and 9 encompass various aspects of the system, including captured CO_2 (547.5–1,169.8 kg) and electricity usage in the CCS subsystem

Table 3
Design parameters of the CSTGB system in each location.

Location	Location A	Location B	Location C	Location D	Location E	Unit	Adapted based on data from existing studies or calculated
	Lat: 37.5, Lon: –5.3	Lat: 36.6, Lon: –5.8	Lat: 39.9, Lon: –5.7	Lat: 39.2, Lon: –3.3	Lat: 38.7, Lon: –0.9		
Elevation	137	107	272	648	544	m	[18]
Average DNI	641.4	562.7	535.7	542.3	553.7	W/m^2	[18]
Average solar duration	11.2	10.7	10.6	10.8	10.6	hr	[18]
Average ambient temperature	19.1	18.2	15.8	15.6	15.4	°C	[18]
CST receiver specification							
Receiver type	External cylindrical	External cylindrical	External cylindrical	External cylindrical	External cylindrical		[29]
Receiver height	4.8	4.8	4.8	4.8	4.8	m	[29]
Receiver diameter	4.7	4.7	4.7	4.7	4.7	m	[29]
Receiver area	30	30	30	30	30	m^2	[29]
Tower height	80	85	85	85	85	m	calculated
Optical efficiency (at receiver)	71.7	70.2	69.8	65.7	73.8	%	calculated
Designed solar receiver needed temperature	941.6–1,666.5	941.6–1,666.5	941.6–1,666.5	941.6–1,666.5	941.6–1,666.5	°C	calculated
Solar flux concentration ratio	687.7–13,516.6	783.8–15,407.1	823.4–16,183.6	813.3–15,986.7	796.6–15,657.5		calculated
Heliostat specification							
Single heliostat width	12	12	12	12	12	m	[30]
Single heliostat height	10	10	10	10	10	m	[30]
Single heliostat area	120	120	120	120	120	m^2	[30]
Number of single heliostats	240–4,712	274–5,371	288–5,642	284–5,573	278–5,458	unit	calculated
TES specification							
Number of tanks	1	1	1	1	1	Integrated tank	[31,32]
Tank type	External cylindrical	External cylindrical	External cylindrical	External cylindrical	External cylindrical		[31,32]
Tank height	20	19	18.5	18.5	19	m	calculated
Tank diameter (with 0.1 m insulation layer)	10.5	9.5	9.5	10.0	10.0	m	calculated
TES duration	12.8	13.3	13.4	13.2	13.4	hr	calculated
Capacity of the TES	300	265	250	255	260	MW_{th}	calculated
TES heat loss	10	10	10	10	10	%	[33]
Designed Temperature of TES	450	395	375	380	390	°C	calculated
HSM of TES	Quartz sand	Quartz sand	Quartz sand	Quartz sand	Quartz sand		[34]
Total sand weight	1,250	1,100	1,040	1,060	1,080	ton	calculated
Total sand volume	1,660	1,470	1,385	1,415	1,440	m^3	calculated
Gasifier specification							
Gasifier type	Fixed bed	Fixed bed	Fixed bed	Fixed bed	Fixed bed		[31,35]
Gasifier agent	Air (O2:21 %, N2:79 %)	Air (O2:21 %, N2:79 %)	Air (O2:21 %, N2:79 %)	Air (O2:21 %, N2:79 %)	Air (O2:21 %, N2:79 %)		
Pressure	Atmospheric	Atmospheric	Atmospheric	Atmospheric	Atmospheric		
Gasifier heat lose	10	10	10	10	10	%	[33]
Air to feedstock ratio	0.05–0.30	0.05–0.30	0.05–0.30	0.05–0.30	0.05–0.30		calculated
Inlet temperature of quartz sand	856–1,515	856–1,515	856–1,515	856–1,515	856–1,515	°C	calculated
Gasification temperature	678–1,200	678–1,200	678–1,200	678–1,200	678–1,200	°C	calculated
Output temperature of quartz sand	637–1,125	637–1,125	637–1,125	637–1,125	637–1,125	°C	calculated
CCGT specification							
Electricity conversion efficiency[a]	40	40	40	40	40	%	[27]
Efficiency of the CO_2 capture unit	90	90	90	90	90	%	[27,31,36]
Pressure ratio of GT compressor	19	19	19	19	19		[27,31,36]
Turbine inlet temperature	1,288	1,288	1,288	1,288	1,288	°C	[27,31,36]

(*continued on next page*)

Table 3 (*continued*)

Location	Location A	Location B	Location C	Location D	Location E	Unit	Adapted based on data from existing studies or calculated
	Lat: 37.5, Lon: –5.3	Lat: 36.6, Lon: –5.8	Lat: 39.9, Lon: –5.7	Lat: 39.2, Lon: –3.3	Lat: 38.7, Lon: –0.9		
Turbine exhaust temperature	544.2	544.2	544.2	544.2	544.2	°C	[27,31,36]
High-pressure steam	521.2	521.2	521.2	521.2	521.2	°C/55 bar	[27,31,36]
Low-pressure steam	260.2	260.2	260.2	260.2	260.2	°C/6.9 bar	[27,31,36]
Screw machine specification							
Machine-1 for feedstock input							
Screw diameter	1	1	1	1	1	m	[37]
Screw pitch	0.6	0.6	0.6	0.6	0.6	m	[37]
Rotational speed	50	50	50	50	50	rpm	[37]
Conveying capacity	608	608	608	608	608	m^3/h	calculated
Power	96	96	96	96	96	kW	calculated
Machine-2 for sand transfer							
Screw diameter	0.6	0.6	0.6	0.6	0.6	m	[37]
Screw pitch	0.5	0.5	0.5	0.5	0.5	m	[37]
Rotational speed	50	50	50	50	50	rpm	[37]
Conveying capacity	160	160	160	160	160	m^3/h	calculated
Power	159.7	159.7	159.7	159.7	159.7	kW	calculated
Screw pipe specification							
Screw pipe heat loss	10	10	10	10	10	%	[33]
Pipe-1 for feedstock input							
Screw diameter	1	1	1	1	1	m	[37]
Length	30	30	30	30	30	m	calculated
Pipe-2 for sand transfer							
Screw diameter (0.025 m insulation)	0.7	0.7	0.7	0.7	0.7	m	[37]
Length	285	295	295	295	295	m	calculated

[a] Electricity conversion efficiency refers to the CCGT subsystem's capability to convert producer gas into electricity.

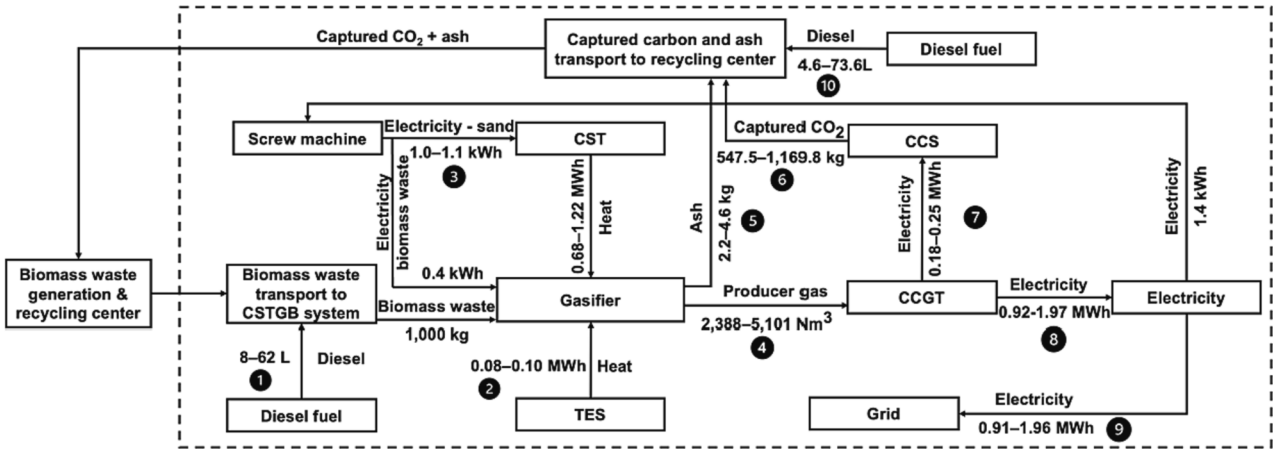

Fig. 5. LCA boundary of the CSTGB system.

(0.18–0.25 MWh), electricity generation from CCGT subsystem (0.92–1.97 MWh), and the subsequent transfer of generated electricity to the grid (0.91–1.96 MWh), with all values subject to LHV and yield of producer gas, the efficiency of the CCGT and CCS subsystem. Lastly, point 10 represents the diesel consumption (4.6–73.6 L) required for transporting captured carbon and ash back to the recycling center. This interconnected system considers various factors to ensure an efficient approach to biomass waste treatment. The entire LCA procedure strictly adheres to the guidelines outlined in ISO 14040 and is executed using the GaBi commercial LCA software [26].

2.5.1. Life cycle inventory

Biomass wastes underwent a drying-pretreatment process and was subsequently transported to the CSTGB system location via trucks. The chemical composition of the biomass waste is detailed in Section 2.2, and it was assumed that the CSTGB system had a processing capacity of 1,700 tons per day. Table 3 shows the specifications of the CSTGB system determined based on factors such as gasification reaction temperature and the local average DNI (as mentioned in Section 2.2). The CST subsystem parameters, including the heliostat field area, receiver area, receiver tower height, and solar thermal efficiency, was optimized using

the SolarPILOT software with default environmental parameters (*i.e.,* incidence angle, ambient humidity, and cloud thickness). The individual heliostat area in the CST subsystem was set at 120 m^2, and the capacity of the TES subsystem was established based on the required peak thermal energy storage for each specific location (as outlined in Section 2.2).

The assumed heat transfer efficiency from quartz sand to the feedstock within the gasifier was set at 100 %. This assumption was made to ensure that the reactions taking place inside the gasifier were in thermal equilibrium, thereby maximizing energy conversion efficiency. The heat transfer efficiency from quartz sand to the feedstock inside the gasifier was assumed to be 100 %. The reactions within the gasifier were in thermal equilibrium, ensuring maximum energy conversion. This resulted in an input temperature range of 856–1,515 °C and an output temperature of 637–1,125 °C for the quartz sand when the gasification reaction temperature was between 678 and 1,200 °C. To convert the producer gas into electricity, a CCGT subsystem with a 40 % electricity conversion efficiency was employed (as mentioned in Table 3) [27]. The CCS equipment consumed 30 % of the gross power output [28].

The CSTGB system incorporated two distinct STMs. Machine I (designed for a transportation distance of 10 m) was responsible for delivering biomass waste to the gasifier. Machine II (designed for a transportation distance of 285, 295, 295, 295, and 295 m for the CSTGB system in location A, B, C, D, and E, respectively) facilitated the movement of quartz sand between the CST, TES, and gasifier subsystems. All subsystems and screw pipelines were assumed that heat losses amounted to 10 % [4].

Table 4 provided a comprehensive breakdown of the material usage for each subsystem of the CSTGB system. To withstand the operational

Table 4
LCI for the construction stage of the CSTGB system is normalized based on the functional unit (*i.e.,* 1 $ton_{biomass\text{-}waste}$) in each location.

Construction materials							
Material type	**Component**	**Location A**	**Location B**	**Location C**	**Location D**	**Location E**	**Unit**
Installation of CST − 120 m^2 heliostat							
Flat glass coated, RER	Flat glass coated, RER	8.1×10^{-2}	9.3×10^{-2}	9.7×10^{-2}	9.6×10^{-2}	9.4×10^{-2}	$kg/ton_{biomass\text{-}waste}$
Reinforcing steel, RER	Reinforcing steel, RER	2.9×10^{-1}	3.3×10^{-1}	3.4×10^{-1}	3.4×10^{-1}	3.3×10^{-1}	$kg/ton_{biomass\text{-}waste}$
Concrete, sole plate and foundation, CH	Concrete foundation	2.1×10^{-4}	2.4×10^{-4}	2.5×10^{-4}	2.5×10^{-4}	2.5×10^{-4}	$m^3/ ton_{biomass\text{-}waste}$
Receiver							
Chromium steel 18/8, RER	Receiver surface	3.2×10^{-4}	3.2×10^{-4}	3.2×10^{-4}	3.2×10^{-4}	3.2×10^{-4}	$kg/ton_{biomass\text{-}waste}$
CST tower							
Tower height		80	85	85	85	85	m
Concrete, sole plate and foundation, CH	Tower concrete	3.3×10^{-4}	3.5×10^{-4}	3.5×10^{-4}	3.5×10^{-4}	3.5×10^{-4}	$m^3/ ton_{biomass\text{-}waste}$
Excavation, hydraulic digger, RER	Tower excavation	2.3×10^{-4}	2.4×10^{-4}	2.4×10^{-4}	2.4×10^{-4}	2.4×10^{-4}	$m^3/ ton_{biomass\text{-}waste}$
Reinforcing steel, RER	Tower steel	6.5×10^{-5}	6.9×10^{-5}	6.9×10^{-5}	6.9×10^{-5}	6.9×10^{-5}	$kg/ton_{biomass\text{-}waste}$
Installation of TES							
Steel, chromium steel 18/8, hot rolled	TES structure	3.1×10^{-2}	3.1×10^{-2}	3.1×10^{-2}	3.1×10^{-2}	3.1×10^{-2}	$kg/ton_{biomass\text{-}waste}$
Stone wool	TES insulation material	1.4×10^{-2}	1.4×10^{-2}	1.4×10^{-2}	1.4×10^{-2}	1.4×10^{-2}	$kg/ton_{biomass\text{-}waste}$
Installation of gasifier							
Reinforcing steel, RER	Steel structure	5.4×10^{-1}	5.4×10^{-1}	5.4×10^{-1}	5.4×10^{-1}	5.4×10^{-1}	$kg/ton_{biomass\text{-}waste}$
Steel, low-alloyed, RER	Steel structure	3.2×10^{-1}	3.2×10^{-1}	3.2×10^{-1}	3.2×10^{-1}	3.2×10^{-1}	$kg/ton_{biomass\text{-}waste}$
Steel, electric, n-and low-alloyed, RER	Steel structure	1.3×10^{-2}	1.3×10^{-2}	1.3×10^{-2}	1.3×10^{-2}	1.3×10^{-2}	$kg/ton_{biomass\text{-}waste}$
Chromium steel 18/8, RER	Steel structure	8.8×10^{-1}	8.8×10^{-1}	8.8×10^{-1}	8.8×10^{-1}	8.8×10^{-1}	$kg/ton_{biomass\text{-}waste}$
Concrete, normal, CH	Concrete foundation	5.1×10^{-3}	5.1×10^{-3}	5.1×10^{-3}	5.1×10^{-3}	5.1×10^{-3}	$m^3/ton_{biomass\text{-}waste}$
Aluminum, secondary, from new scrap, RER	Aluminum structure	5.6×10^{-3}	5.6×10^{-3}	5.6×10^{-3}	5.6×10^{-3}	5.6×10^{-3}	$kg/ton_{biomass\text{-}waste}$
Aluminum, secondary, from old scrap, RER	Aluminum structure	2.8×10^{-3}	2.8×10^{-3}	2.8×10^{-3}	2.8×10^{-3}	2.8×10^{-3}	$kg/ton_{biomass\text{-}waste}$
Aluminum, primary, RER	Aluminum structure	4.8×10^{-2}	4.8×10^{-2}	4.8×10^{-2}	4.8×10^{-2}	4.8×10^{-2}	$kg/ton_{biomass\text{-}waste}$
Brass, CH	Plant material	5.8×10^{-3}	5.8×10^{-3}	5.8×10^{-3}	5.8×10^{-3}	5.8×10^{-3}	$kg/ton_{biomass\text{-}waste}$
Stone wool, CH	Insulation material	9.3×10^{-2}	9.3×10^{-2}	9.3×10^{-2}	9.3×10^{-2}	9.3×10^{-2}	$kg/ton_{biomass\text{-}waste}$
Glass fiber, RER	Plant material	1.3×10^{-2}	1.3×10^{-2}	1.3×10^{-2}	1.3×10^{-2}	1.3×10^{-2}	$kg/ton_{biomass\text{-}waste}$
Polyvinyl, HDPE, granulate, RER	Plant material	3.7×10^{-3}	3.7×10^{-3}	3.7×10^{-3}	3.7×10^{-3}	3.7×10^{-3}	$kg/ton_{biomass\text{-}waste}$
Polypropylene, granulate, RER	Plant material	1.9×10^{-3}	1.9×10^{-3}	1.9×10^{-3}	1.9×10^{-3}	1.9×10^{-3}	$kg/ton_{biomass\text{-}waste}$
Styrene-acrylonitrile copolymer, RER	Plant material	6.2×10^{-4}	6.2×10^{-4}	6.2×10^{-4}	6.2×10^{-4}	6.2×10^{-4}	$kg/ton_{biomass\text{-}waste}$
Flat glass, uncoated, RER	Plant material	6.3×10^{-4}	6.3×10^{-4}	6.3×10^{-4}	6.3×10^{-4}	6.3×10^{-4}	$kg/ton_{biomass\text{-}waste}$
Cast iron, RER	Plant material	2.3×10^{-2}	2.3×10^{-2}	2.3×10^{-2}	2.3×10^{-2}	2.3×10^{-2}	$kg/ton_{biomass\text{-}waste}$
Epoxy resin, liquid, RER	Plant material	4.9×10^{-3}	4.9×10^{-3}	4.9×10^{-3}	4.9×10^{-3}	4.9×10^{-3}	$kg/ton_{biomass\text{-}waste}$
Lubricating oil, RER	Plant material	2.1×10^{-2}	2.1×10^{-2}	2.1×10^{-2}	2.1×10^{-2}	2.1×10^{-2}	$kg/ton_{biomass\text{-}waste}$
Synthetic rubber, RER	Producer gas pipe	2.8×10^{-3}	2.8×10^{-3}	2.8×10^{-3}	2.8×10^{-3}	2.8×10^{-3}	$kg/ton_{biomass\text{-}waste}$
Installation of CCGT							
Reinforcing steel, RER	Steel structure	6.8	6.8	6.8	6.8	6.8	$kg/ton_{biomass\text{-}waste}$
Chromium steel 18/8, RER	Steel structure	8.7×10^{-3}	8.7×10^{-3}	8.7×10^{-3}	8.7×10^{-3}	8.7×10^{-3}	$kg/ton_{biomass\text{-}waste}$
Aluminum, RER	Aluminum structure	4.4×10^{-3}	4.4×10^{-3}	4.4×10^{-3}	4.4×10^{-3}	4.4×10^{-3}	$kg/ton_{biomass\text{-}waste}$
Concrete, sole plate and foundation, CH	Concrete foundation building	2.1	2.1	2.1	2.1	2.1	$kg/ton_{biomass\text{-}waste}$
Installation of pipes							
Pipe length		315	325	325	325	325	m
Reinforcing steel, RER	Steel pipe	1.0×10^{-2}	1.1×10^{-2}	1.1×10^{-2}	1.1×10^{-2}	1.1×10^{-2}	$kg/ton_{biomass\text{-}waste}$
Stone wool, RER	Insulation material	9.6×10^{-6}	9.6×10^{-6}	9.6×10^{-6}	9.6×10^{-6}	9.6×10^{-6}	$kg/ton_{biomass\text{-}waste}$

temperature of 637–1,515 °C in the CST receiver and CCGT subsystem, chromium steel (with melting point of 1,860 °C) was applied as the construction material. The TES subsystem, gasifier, and screw pipe were meticulously fabricated by using reinforcing steel (it has high melting point of 1,370 °C). Material losses during construction, power consumption during assembling, and emissions and energy consumption associated with demolition of the CSTGB system were omitted. Research has shown that their influence on emissions and energy is minimal compared to the operation phase [38].

2.5.2. Life cycle impact assessment

A life cycle impact assessment (LCIA) was carried out to calculate the selected environmental impact indictors. The LCIA process involved the organization of LCI data into specific impact categories and corresponding indicators, which provide insight into the cause-and-effect relationship between the system's activities and environmental consequences. To calculate the overall GWP of the CSTGB system, *i.e.*, GHG emissions associated with the system over a 100-year period (referred to as GWP 100 horizon), the ReCiPe Midpoint V1.08 methodology was employed [4].

2.6. Techno-economic analysis

The economic feasibility of the proposed CSTGB system was evaluated using the NPW approach. This process entailed a detailed examination of all financial transactions linked to the CSTGB system proposal over a 30-year duration, where each cash flow was converted into its equivalent present worth (PW). Positive cash flows were attributed to revenues, while negative cash flows were associated with costs [39]. The net present worth (NPW) of the system was calculated by

$$NPW = CAPEX + PW(O\&M) + PW(T) - PW(ES) - PW(CT) \quad (2)$$

where CAPEX represents the capital cost, which covers the initial investment required for establishing the CSTGB system. O&M represents the operational and maintenance costs, while T accounts for the expenses associated with transporting feedstock from Sevilla to the CSTGB system site. ES is the notation for the revenue obtained through the sale of renewable electricity, and CT denotes the income generated from carbon tax. The calculation of the PW is determined by annual worth (AW):

$$PW = AW\frac{(1+i)^N - 1}{i(1+i)^N} \quad (3)$$

where i represents the interest rate with a rate of 6 % utilized in accordance with literature [39]. N signifies the assumed operation years, which was set at 30 years for this study. Furthermore, the currency exchange rate was 1.13 euros to US dollar and 0.85 British pounds to US dollars as the year 2019.

The process costing method was employed to compute the CAPEX for each subsystem within the proposed CSTGB system, specifically the CST, gasifier, and CCGT. These individual CAPEX values were then aggregated to determine the total CAPEX [4]. To standardize the CAPEX of each subsystem to the reference year 2019 (with a CEPCI index of 556.8 [40]), the Chemical Engineering Plant Cost Index (CEPCI) data were used and implemented Eq. (4).

$$Cost_{ref} = Cost_{base}\left(\frac{CEPCI_{ref}}{CEPCI_{base}}\right) \quad (4)$$

Table 5 presents a comprehensive consolidation of the CAPEX, which includes costs related to truck acquisitions (determined by the transportation distances), along with the O&M cost and revenues generation for the CSTGB system at different locations. The CAPEX for a single heliostat was calculated as €103 it was referred by a cost of €112.4 [30] at the year 2015 (with a CEPCI index of 556.8 [40]). The calculation of the O&M cost for the CST subsystem is based on the data from 100 MW-scale system published by International Renewable Energy Agency (IRENA) in 2018 (with a CEPCI index of 603.1 [40]). It encompasses costs related to the receiver, tower, TES, and indirect expense (*i.e.,* owner costs, contingency, and site preparation). These costs are summed and then divided by the total electricity generation capacity of the system to determine the annual O&M cost of the CST subsystem as 17.8 €/MWh. The CAPEX for the gasifier and CCGT subsystem was calculated based on the 2008 (with a CEPCI index of 575 [40]) report from the National Renewable Energy Laboratory (NREL) [41]. The CAPEX includes the costs for gas clean-up facilities, engineering expenses, contingencies, and carbon capture cost. The O&M cost for the integrated

Table 5
CAPEX, O&M, and transportation costs for the CSTGB system at each location.

	Location A	Location B	Location C	Location D	Location E	Unit	Ref(s)
CAPEX							
CST subsystem							
Heliostat field	0.02–0.5	0.03–0.55	0.03–0.58	0.03–0.57	0.03–0.56	million €	[30]
Receiver	52.9	52.9	52.9	52.9	52.9	million €	[46]
Receiver tower	26.9	28.5	28.5	28.5	28.5	million €	[47]
TES	74.6	65.9	62.2	63.4	64.7	million €	[47]
Gasifier + CCGT subsystems							
Gasifier	60.2	60.2	60.2	60.2	60.2	million €	[41]
CCGT	111.8	111.8	111.8	111.8	111.8	million €	[41]
Site preparation	4.3–83.5	4.9–95.2	5.1–100.0	5.0–98.7	4.9–96.7	million €	[41]
Indirect costs	21.3–417.5	24.3–475.9	25.5–499.8	25.2–493.8	24.6–483.6	million €	[41]
O&M costs							
CST subsystem	17.8	17.8	17.8	17.8	17.8	€/MWh	[41,48,49]
Gasifier + CCGT subsystem	12.7	12.7	12.7	12.7	12.7	€/MWh	[41,48,49]
CCS device	23.7	23.7	23.7	23.7	23.7	€/MWh	[41,48,49]
Transportation costs							
Number of trucks	17	34	136	136	136	unit	calculated
Number of staffs	51	102	408	408	408	unit	calculated
CAPEX of trucks (10 years)	3.9	7.9	31.7	31.7	31.7	million €	[39,43]
O&M cost of trucks	7	13	52	52	52	€/hour	[39,43]
Diesel cost	1785	3570	14,280	14,280	14,280	€/hour	calculated
Staff cost	6120	12,240	48,960	48,960	48,960	€/hour	calculated

gasifier and CCGT as 36.4 €/MWh was referred from [42] for the year 2019. The total O&M cost for the entire CSTGB system accounted for the CST, gasifier, and CCGT subsystem and was equal to 54.2 €/MWh. Transportation costs encompass the acquisition of trucks (233,335 €/truck with a 10-year lifespan with an annual O&M cost is 3,335 €/truck [39]), diesel cost as 1.26 €/L [4], and the wages of truck operator (15.0 €/h/person working 8 h/day [43]) in the 2019. The ES price in Spain was determined at 50 €/MWh, following the Feed-in Tariff (FiT). It incorporated taxes for electricity generated from renewable sources [44]. Additionally, the CT in Spain is established at 49 €/tCO_2 [45] and used in the TEA of the proposed CSTGB system.

2.7. Multi-objective optimization

One of the most crucial and prevalent challenges lies in addressing multiple conflicting objectives in designing the CSTGB system, which requires simultaneous resolution. The pursuit of a more efficient energy system invariably results in augmented costs for both system components and the entirety of the system. Within the domain of MOO techniques, this study leveraged the LSTM-RNN model in conjunction with the LCA and TEA methodologies to derive and compile a comprehensive set of 280,000 scenarios in this study. These scenarios collectively embody values related to system performance, GWP, and NPW. The identification of the best scenario possessing such attributes substantially facilitates the design of the CSTGB system, enabling its operation in a state that optimizes efficiency, environmental viability, and economic feasibility to the utmost degree.

Two antagonistic objectives are postulated for optimization: to minimize GWP as a representative of the carbon footprint metric, and to simultaneously maximize NPW as an economic indicator that also encompasses the performance metric of electricity generation. In pursuit of these goals, this study deployed the pareto optimality and the TOPSIS method. The pareto optimality method identified scenarios where NPW can be elevated without detriment to GWP. Meanwhile, the TOPSIS method comprehensively assesses the divergence between pareto optimal solutions and the ideal best solution. It could provide a ranked selection avenue for multi-objective decision-making. This combination of techniques holistically explores trade-offs across manifold objectives within the CSTGB system design, thereby identifying optimal scenario design parameters, and associated GWP and NPW values.

3. Results and discussion

3.1. Forecasting of electricity generation and carbon saving by CSTGB system

The kinetic model of CSTGB exhibited a simulation error rate below 12 % and reasonably characterize the thermochemical process of gasification as highlighted in the previous paper [4,16]. As this work focuses on system optimization based on the comparison of different scenarios predicted based on the same model, it is believed the absolute accuracy of the model should have a limited impact on the selection of optimal solutions. These input variables can be subject to external influences (*i.e.,* location), which not only adds complexity and uncertainty to the resulting outcomes but also hinders the training of the LSTM-RNN model. Therefore, we have chosen to use intermediate variables (*i.e.,* electricity generation and CO_2 captured) as the output results for the LSTM-RNN model. This decision aims to better capture critical aspects of system performance and mitigate the impact of external factors on the analysis. Moreover, sensitivity analysis demonstrated that the electricity generation and CO_2 captured have a substantial impact on the outcomes of LCA and TEA [4]. Higher levels of electricity generation are inherently linked to greater energy output and revenue generation, while increased carbon capture contributes to reducing CO_2 emissions and potential carbon saving.

Fig. 6 serves as an illustrative representation of mean values pertaining to annual electricity generation and carbon capture across various biomass waste types, temperature gradations, and geographical locales. The length of each bar correlates directly to mean values within specific parameter combinations. Analysis of mean values shows a

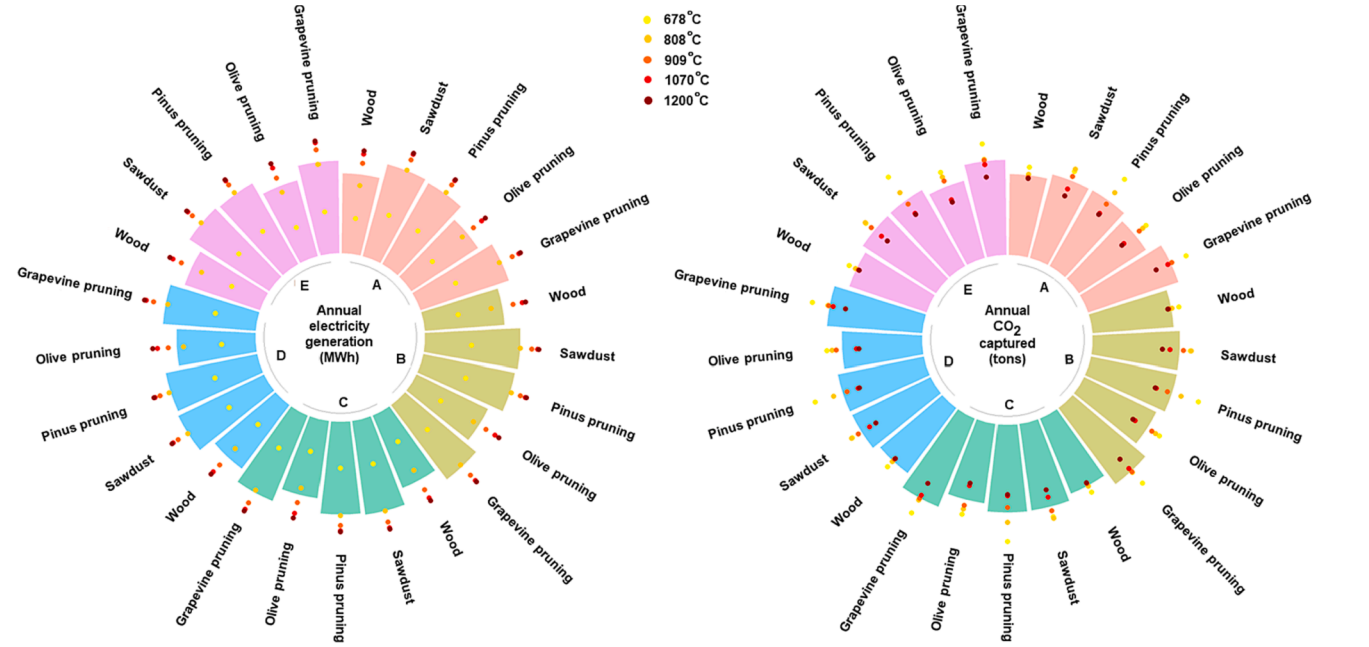

Annual electricity generation (MWh)

	Location A	Location B	Location C	Location D	Location E
Wood waste	9.5×10^5	9.5×10^5	9.3×10^5	9.4×10^5	9.4×10^5
Sawdust waste	1.1×10^6	1.1×10^6	1.1×10^6	1.1×10^6	1.1×10^6
Pinus pruning waste	1.1×10^6	1.1×10^6	1.1×10^6	1.1×10^6	1.1×10^6
Olive pruning waste	9.4×10^5	9.4×10^5	9.3×10^5	9.4×10^5	9.3×10^5
Grapevine pruning waste	1.1×10^6	1.1×10^6	1.1×10^6	1.1×10^6	1.1×10^6

Annual CO_2 captured (tons)

	Location A	Location B	Location C	Location D	Location E
Wood waste	9.3×10^5	9.3×10^5	9.3×10^5	9.3×10^5	9.3×10^5
Sawdust waste	9.9×10^5	1.0×10^6	1.0×10^6	1.0×10^6	1.0×10^6
Pinus pruning waste	1.0×10^6	1.0×10^6	1.0×10^6	1.0×10^6	1.0×10^6
Olive pruning waste	9.1×10^5	9.1×10^5	9.2×10^5	9.2×10^5	9.2×10^5
Grapevine pruning waste	1.1×10^6	1.1×10^6	1.1×10^6	1.1×10^6	1.1×10^6

Fig. 6. 125 scenarios set descriptive statistics.

consistent trend, revealing that sawdust waste yields the highest annual electricity generation, closely trailed by grapevine pruning waste, pinus pruning waste, wood waste, and olive pruning waste. This observation suggests that sawdust and grapevine pruning waste promise as potent options for electricity generation within the considered waste types (as detailed in Section 2.2 outlining feedstock composition) in the CSTGB system.

Further analysis extends to the impact of varying operating temperatures on energy generation and CO_2 capture efficacy. With increasing temperatures, annual electricity generation demonstrates an ascending trajectory, whereas carbon capture exhibits a descent, irrespective of the biomass waste type. Importantly, this trend maintains consistency across all evaluated biomass waste types.

Expanding the analysis to encompass geographical location, discernible fluctuations in annual electricity generation were found. Location A consistently emerges as the lead in mean electricity generation, followed by Location B, Location C, Location D, and Location E. The fundamental reason or factor of this divergence can be traced to the superior local climate conditions prevalent at Location A. These conditions, typified by the highest average DNI of 641.4 W/m^2, minimal average wind speed of 3 km/h, lowest average precipitation of 53.4 mm/month, and elevated environmental temperatures 19 °C, collectively contribute to its higher electricity generation. In summary, the zenith of the system performance is attained through the utilization of sawdust waste as the feedstock, operation at 1,200 °C, and positioning at location A within the scope of 125 scenarios. Within these scenarios, the overall system efficiency (a metric for assessing the energy conversion efficiency from biomass and solar energy to electricity) exhibits a range from 9.10 % to 51.59 %. This variation underscores the system's adaptability and the impact of operational conditions on the overall energy conversion efficiency.

3.2. Performance evaluation of LSTM-RNN model

Fig. 7A represented the evaluation of the LSTM-RNN model, and a distinct trend was observed whereby the MSE exhibited rapid reduction within the 1st to 5th epochs. This signifies the model's ability to assimilate underlying data patterns and features during its learning phase. After the 10th epoch, the MSE stabilizes at values of 29.4 and 9.2 for the training and validation processes, respectively.

In assessing the performance of the model, the LSTM-RNN model was employed to predict electricity generation (Fig. 7B) and carbon savings, (Fig. 7C) and the resultant predictions were validated against the corresponding test data. The predictive outcomes closely matched the testing data, as indicated by an average error of 5.16 %.

3.3. Evaluation of MOO results

A comprehensive exploration of 280,000 scenarios was undertaken using the MOO method. It is essential to emphasize that negative values were employed for the GWP metric in Fig. 8. A lower GWP signified a higher level of CO_2 capture in the CSTGB system, indicative of a decreased efficiency of the CSTB system and a greater emission of CO_2. The inclusion of the CT in the analysis had a significant impact on the MOO results. Due to the CSTGB system was maintained under an assumption that does not account for market supply and demand interactions (refers to the availability of electricity in response to market demand) on calculating the NPW. This circumstance might have led to a greater influence of the CT on the system revenue. This phenomenon aligns with the findings of research regarding the CT by [50], where they asserted that the CT tend to amplify the revenue of relevant systems.

Fig. 8A illustrated the influence of incorporating the CT in the TEA on the MOO outcomes of the CSTGB system. This incorporation led to the absence of trade-off in the MOO results. Consequently, this enabled the swift determination of the best scenario, even in the absence of using the pareto optimality and TOPSIS methods. In the parameter configuration of the best scenario, the feedstock composition played a crucial role in the system efficiency: C (49.3 wt%), H (7.3 wt%), O (42.4 wt%), N (0.9 wt%), FC (18.1 wt%), and the feedstock LHV (18.5 kJ/kg). The optimal conditions converged at Location C, and the CSTGB system with

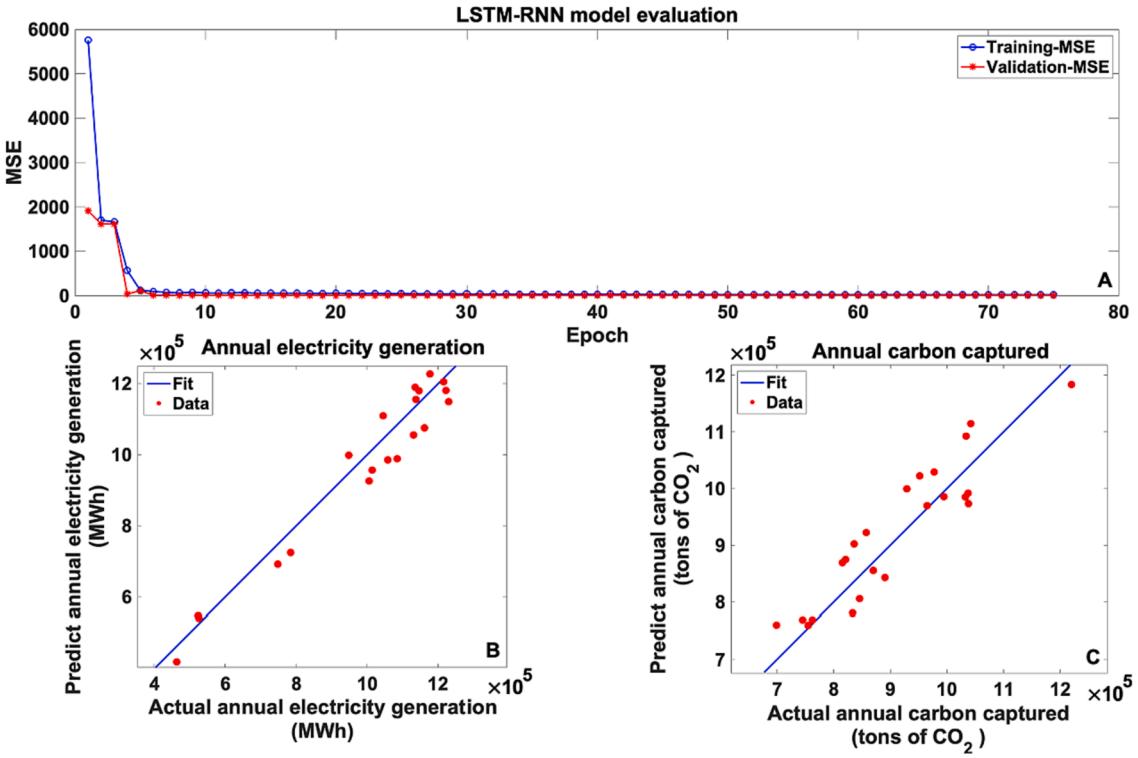

Fig. 7. (A). the proposed LSTM-RNN model evaluation, (B). comparison of predict and actual annual electricity generation, (C). comparison of predict and actual annual carbon captured.

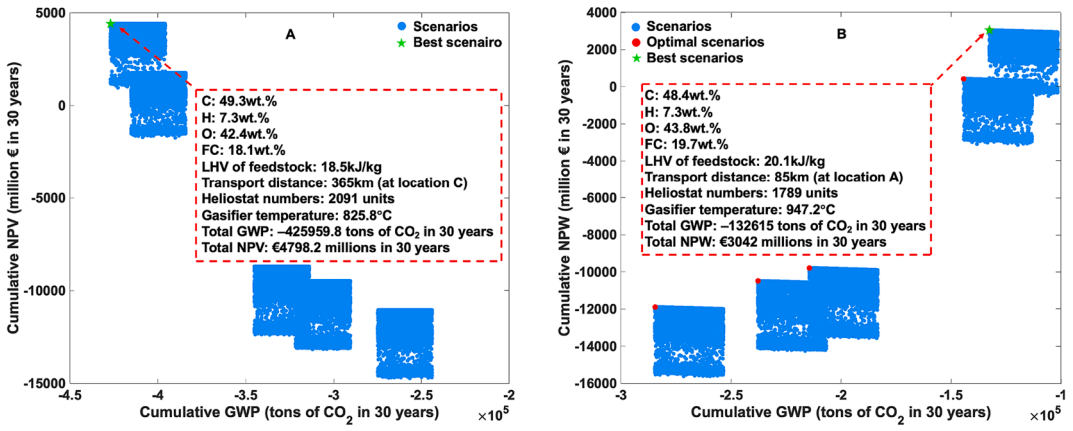

Fig. 8. The decision making of the optimal scenario: A). the CSTGB system with considered CT as revenue, B). the CSTGB system without considered CT as revenue.

2091 heliostats operated at a gasification temperature condition of 825.8 °C. Over the span of 30 years, the cumulative GWP reduction amounted to 415,960 tons CO_2-eq. TEA presented promising cost-effective results with NPW of €4,298 million. A key correlation emerged between the CT revenue and the extent of CO_2 captured, creating a symbiotic relationship: increasing CO_2 captured capacity led to increased CT revenue. The optimal process correspond to the operation at lower reaction temperatures and established at Location C (characterized by the lowest average DNI of 535.7 W/m^2 and a longer transportation distance of 365 km).

Fig. 8B illustrated the impact of incorporating CT in the TEA on the MOO results of the CSTGB system. Optimal scenarios were determined by using the pareto optimality and the TOPSIS method was used to make a decision of the most preferred system scenario. The best system scenario was determined as: C (48.4 wt%), H (7.3 wt%), O (43.8 wt%), FC (19.7 wt%), the feedstock LHV (20.1 kJ/kg), and location A, which is attributed to that location A has the shortest transportation distance (85 km) and the highest average DNI (641.4 W/m^2). This location choice integrates the transport efficiency and the availability of solar energy resources, aligning with system objectives (*e.g.,* specifically the maximization of NPW and the minimization of GWP). The optimal number of heliostats was 1,789, associated with a gasification temperature of 947.2 °C. Over a 30-year lifecycle, the cumulative reduction in GWP amounted to 132,615 tons CO_2-eq. This aligns closely with the pressing global environmental imperatives, underscoring the system's potential role in carbon emission mitigation. The TEA also demonstrated prospects, as reflected by the substantial NPW of €3,042 million.

4. Conclusion

In the pursuit of optimizing the economics and carbon saving potential of CSTGB systems, an analysis of diverse influencing factors has been undertaken. This has revealed insights that pave the way for efficient and sustainable energy production strategies. The data associated with 125 scenarios were gathered for training the LSTM-RNN model that predicts electricity generation and carbon captured with an error of 5.1 %. Subsequently, the LSTM-RNN model was utilized to extend these 125 scenarios to create 280,000 datasets using the Monte Carlo simulation approach for MOO. Within the MOO framework, the influences of various parameters of the CSTGB system, such as the feedstock composition, operating temperature, and location of the CSTGB system towards GWP and NPW were examined. This study not only underscored the system's potential for enhanced efficiency and emissions reduction but also emphasized its economic potential. Particularly significant was the impact of the CT on MOO results. The optimal configuration of the system could avoid the trade-off phenomenon when treating the CT as a revenue. The most favorable scenario demonstrated a significant reduction in GWP, achieving a cumulative saving of 415,960 tons of CO_2-eq and NPW of €4,298 million over a 30-year lifespan when CT was accounted for as a revenue. A scenario excluding CT corresponded to a reduction of 132,615 tons of CO_2-eq and an NPW of €3,042 million. This finding demonstrates the significance in the consideration of multifaceted factors in decision-making, synergizing technological innovation, economic benefits, and environmental impacts.

CRediT authorship contribution statement

Yi Fang: Conceptualization, Data curation, Formal analysis, Investigation, Writing – original draft. **Xian Li:** Data curation, Writing – review & editing. **Xiaonan Wang:** Funding acquisition, Supervision, Writing – review & editing. **Leilei Dai:** Writing – review & editing. **Roger Ruan:** Writing – review & editing. **Siming You:** Funding acquisition, Supervision, Writing – review & editing.

Declaration of competing interest

The authors declare that they have no known competing financial interests or personal relationships that could have appeared to influence the work reported in this paper.

Data availability

All data supporting this study are provided in full in the paper.

Acknowledgements

Siming You acknowledges the Engineering and Physical Sciences Research Council (EPSRC) Programme Grant (EP/V030515/1). This project was also partially funded by the European Union's Horizon 2020 research and innovation programme under the Marie Sklodowska-Curie grant agreement No. 101007976. Xiaonan Wang acknowledges the financial support from the National Key R&D Program of China (2023YFE0204600). All data supporting this study are provided in full in the paper.

References

[1] Li X, Chen J, Hu Q, Chu P, Dai Y, Wang C-H. Solar-driven gasification in an indirectly-irradiated thermochemical reactor with a clapboard-type internally-circulating fluidized bed. Energ Conver Manage 2021;248:114795.
[2] Fang Y, Paul MC, Varjani S, Li X, Park Y-K, You S. Concentrated solar thermochemical gasification of biomass: Principles, applications, and development. Renew Sustain Energy Rev 2021;150:111484.
[3] Fthenakis V, Frischknecht R, Raugei M, Kim HC, Alsema E, Held M, et al. Methodology guidelines on life cycle assessment of photovoltaic electricity. IEA PVPS Task 2011;12.

[4] Fang Y, Li X, Ascher S, Li Y, Dai L, Ruan R, et al. Life cycle assessment and cost benefit analysis of concentrated solar thermal gasification of biomass for continuous electricity generation. Energy 2023.
[5] Wang Z, Li J, Rangaiah GP, Wu Z. Machine learning aided multi-objective optimization and multi-criteria decision making: Framework and two applications in chemical engineering. Comput Chem Eng 2022;165:107945.
[6] Musharavati F, Khoshnevisan A, Alirahmi SM, Ahmadi P, Khanmohammadi S. Multi-objective optimization of a biomass gasification to generate electricity and desalinated water using Grey Wolf Optimizer and artificial neural network. Chemosphere 2022;287:131980.
[7] Gao Z, Miao J, Zhao J, Mesri M. Comprehensive economic analysis and multi-objective optimization of an integrated gasification power generation cycle. Process Saf Environ Prot 2021;155:61–79.
[8] Bouktif S, Fiaz A, Ouni A, Serhani MA. Multi-sequence LSTM-RNN deep learning and metaheuristics for electric load forecasting. Energies 2020;13:391.
[9] Pravin P, Tan JZM, Yap KS, Wu Z. Hyperparameter optimization strategies for machine learning-based stochastic energy efficient scheduling in cyber-physical production systems. Digital Chem Eng 2022;4:100047.
[10] Bishnu SK, Alnouri SY, Al Mohannadi DM. Computational applications using Data Driven Modeling in Process Systems: A Review. Digital Chem Eng. (2023) 100111.
[11] Wagner MJ, Wendelin T. SolarPILOT: A power tower solar field layout and characterization tool. Sol Energy 2018;171:185–96.
[12] Liu J, Huang X, Li Q, Chen Z, Liu G, Tai Y. Hourly stepwise forecasting for solar irradiance using integrated hybrid models CNN-LSTM-MLP combined with error correction and VMD. Energ Conver Manage 2023;280:116804.
[13] Yang L, Zhang X, Liu S, Yu L, Zhang W. Field test of large-scale hydrogen manufacturing from underground coal gasification (UCG). Int J Hydrogen Energy 2008;33:1275–85.
[14] Yin R, Liu R, Wu J, Wu X, Sun C, Wu C. Influence of particle size on performance of a pilot-scale fixed-bed gasification system. Bioresour Technol 2012;119:15–21.
[15] Lü X, Wu Y, Lian J, Zhang Y, Chen C, Wang P, et al. Energy management of hybrid electric vehicles: A review of energy optimization of fuel cell hybrid power system based on genetic algorithm. Energ Conver Manage 2020;205:112474.
[16] Fang Y, Ma L, Yao Z, Li W, You S. Process optimization of biomass gasification with a Monte Carlo approach and random forest algorithm. Energ Conver Manage 2022;264:115734.
[17] Lapuerta M, Hernández JJ, Pazo A, López J. Gasification and co-gasification of biomass wastes: Effect of the biomass origin and the gasifier operating conditions. Fuel Process Technol 2008;89:828–37.
[18] E. Commission. Photovoltaic Geographical Information System (PVGIS).
[19] Wang F, Xuan Z, Zhen Z, Li K, Wang T, Shi M. A day-ahead PV power forecasting method based on LSTM-RNN model and time correlation modification under partial daily pattern prediction framework. Energ Conver Manage 2020;212:112766.
[20] Bottou L. Stochastic gradient learning in neural networks. Proc Neuro-Nımes 1991;91:12.
[21] Qiu B, Huang Z, Liu X, Meng X, You Y, Liu G, et al. Noise reduction in optical coherence tomography images using a deep neural network with perceptually-sensitive loss function. Biomed Opt Express 2020;11:817–30.
[22] Zahra MM, Essai MH, Abd Ellah AR. Performance functions alternatives of MSE for neural networks learning. Int J Eng Res Technol (IJERT) 2014;3:967–70.
[23] Amidi A, Amidi S. Vip cheatsheet: Recurrent neural networks. Stanford University Stanford, CA, USA2018.
[24] Wang M, Yu H, Jing R, Liu H, Chen P, Li C. Combined multi-objective optimization and robustness analysis framework for building integrated energy system under uncertainty. Energ Conver Manage 2020;208:112589.
[25] Arvanitoyannis IS. ISO 14040: life cycle assessment (LCA)–principles and guidelines. In: Waste management for the food industries; 2008. p. 97–132.
[26] Gupta R, Miller R, Sloan W, You S. Economic and environmental assessment of organic waste to biomethane conversion. Bioresour Technol 2022;345:126500.
[27] Baratieri M, Baggio P, Bosio B, Grigiante M, Longo G. The use of biomass syngas in IC engines and CCGT plants: a comparative analysis. Appl Therm Eng 2009;29:3309–18.
[28] PIHL E. Reducing Carbon Emissions From Natural Gas-fired Power Plants. (2012).
[29] Kuenlin A, Augsburger G, Gerber L, Maréchal F. Life cycle assessment and environomic optimization of concentrating solar thermal power plants. 26th international conference on efficiency, cost, optimization, simulation and environmental impact of energy systems (ECOS2013). 2013.
[30] Bhargav K, Gross F, Schramek P. Life Cycle cost optimized heliostat size for power towers. Energy Procedia 2014;49:40–9.
[31] Singh B, Strømman AH, Hertwich E. Life cycle assessment of natural gas combined cycle power plant with post-combustion carbon capture, transport and storage. Int J Greenhouse Gas Control 2011;5:457–66.
[32] Gasa G, Lopez-Roman A, Prieto C, Cabeza LF. Life cycle assessment (LCA) of a concentrating solar power (CSP) plant in tower configuration with and without thermal energy storage (TES). Sustainability 2021;13:3672.
[33] Piatkowski N, Wieckert C, Weimer AW, Steinfeld A. Solar-driven gasification of carbonaceous feedstock—a review. Energ Environ Sci 2011;4:73–82.
[34] Abe T, Gokon N, Izawa T, Kodama T. Internally-circulating fluidized bed reactor using thermal storage material for solar coal coke gasification. Energy Procedia 2015;69:1722–30.
[35] Milani R, Szklo A, Hoffmann BS. Hybridization of concentrated solar power with biomass gasification in Brazil's semiarid region. Energ Conver Manage 2017;143:522–37.
[36] Rubin ES, Chen C, Rao AB. Cost and performance of fossil fuel power plants with CO_2 capture and storage. Energy Policy 2007;35:4444–54.
[37] Screw transfer machine: https://www.alibaba.com/product-detail/Hot-sale-auger-screw-conveyor-for_62166933656.html?spm=a2700.7724857.0.0.128279bbpq1HUB.
[38] Ramachandran S, Yao Z, You S, Massier T, Stimming U, Wang C-H. Life cycle assessment of a sewage sludge and woody biomass co-gasification system. Energy 2017;137:369–76.
[39] Ascher S, Li W, You S. Life cycle assessment and net present worth analysis of a community-based food waste treatment system. Bioresour Technol 2020;305:123076.
[40] Jenkins S. The Chemical Engineering Plant Cost Index.
[41] Craig KR, Mann MK. Cost and performance analysis of biomass-based integrated gasification combined-cycle (BIGCC) power systems. National Renewable Energy Lab.(NREL), Golden, CO (United States)1996.
[42] Cormos A-M, Cormos C-C. Techno-economic assessment of combined hydrogen & power co-generation with carbon capture: The case of coal gasification. Appl Therm Eng 2019;147:29–39.
[43] Mahajan K, Velaga NR, Kumar A, Choudhary A, Choudhary P. Effects of driver work-rest patterns, lifestyle and payment incentives on long-haul truck driver sleepiness. Transport Res F: Traffic Psychol Behav 2019;60:366–82.
[44] Solar T. Solar Panels in Spain: facts, tariffs, development, financing. (2023).
[45] Ortega-Izquierdo M, del Río P. Benefits and costs of renewable electricity in Europe. Renew Sustain Energy Rev 2016;61:372–83.
[46] Turchi CS, Boyd M, Kesseli D, Kurup P, Mehos MS, Neises TW, et al. CSP systems analysis-final project report. National Renewable Energy Lab.(NREL), Golden, CO (United States) (2019).
[47] Zhuang X, Xu X, Liu W, Xu W. LCOE analysis of tower concentrating solar power plants using different molten-salts for thermal energy storage in China. Energies 2019;12:1394.
[48] Kanniche M, Bouallou C. CO_2 capture study in advanced integrated gasification combined cycle. Appl Therm Eng 2007;27:2693–702.
[49] Descamps C, Bouallou C, Kanniche M. Efficiency of an Integrated Gasification Combined Cycle (IGCC) power plant including CO2 removal. Energy 2008;33:874–81.
[50] Burnette SD. A Cost-benefit Analysis of the Australian Carbon Tax and the Economics of. Clim Change 2015.